

ZnSn(OH)₆ nanocubes as a high-performance anode for lithium-ion batteries

Qian Yang¹, Zhibin Wu^{2,3*}, Zhijian Wang¹, Wei Liu¹, Jianwen Liu¹, Chuanqi Feng¹, Wei Sun⁴, Haimin Zhao⁴, Zaiping Guo^{1,2,3}

¹Hubei Collaborative Innovation Centre for Advanced Organic Chemical Materials and Ministry-of-Education Key Laboratory for Synthesis and Applications of Organic Functional Molecules, Hubei University, Wuhan 430062, China

²School of Mechanical, Materials & Mechatronics Engineering, University of Wollongong, Wollongong, New South Wales 2500, Australia

³Institute for Superconducting & Electronic Materials, University of Wollongong, Wollongong, New South Wales 2522, Australia

⁴Tianneng Battery Group Co. Ltd, 18 Baoqiao Road, Huaxi Industrial Functional Zone, Changxing, Zhejiang, 313100, China

*Corresponding author

DOI: 10.5185/amlett.2018.2143

www.vbripress.com/aml

Abstract

Single-phase bi-metal oxides and sulfides have attracted considerable research interest recently for battery application because of their outstanding electrochemical properties, but there are few reports on single-phase bi-metal hydroxides in battery research. Herein, we pioneer the electrochemical study of ZnSn(OH)₆ nanocubes for lithium-ion battery application. The ZnSn(OH)₆ nanocubes, synthesized by a facile hydrothermal method, can deliver a favorable specific discharge capacity of 599.3 mA h g⁻¹ at 500 mA g⁻¹ after 200 cycles and maintain good rate capability even at 2 A g⁻¹. The excellent electrochemical performance of these ZnSn(OH)₆ nanocubes can be attributed to the synergetic Li storage capability of Zn and Sn elements with diverse electrochemical reactions, the small uniform nanocubes (30–50 nm) that alleviate the pulverization and cracking of the electrode and shorten electron/ion transport paths, and the good mechanical properties of ZnSn(OH)₆, which facilitate maintenance of the structural integrity of the electrode during the Li⁺ extraction/insertion process. Therefore, with these outstanding advantages, the ZnSn(OH)₆ nanocubes could be one of the most promising anodes for advanced lithium-ion batteries. Copyright © 2018 VBRI Press.

Keywords: ZnSn(OH)₆, bi-metal hydroxides, lithium-ion batteries, anode.

Introduction

Recently, lithium-ion batteries (LIBs) have become the primary energy supplies for high-technology portable devices and are being actively applied to propel electric vehicles[1]. Although graphite anodes have been widely used in LIBs for commercial mobile devices, their relatively low theoretical capacity (372 mA h g⁻¹) has restricted their practical battery application[2]. Therefore, it is quite an urgent matter to explore novel battery materials with larger theoretical capacity to satisfy the increasing demand for energy storage[3].

In past decades, transition metal oxides (TMOs) have been considered as a class of popular anode material for LIBs because of their high theoretical capacity, natural abundance, and environmental friendliness. Their practical use was limited, however, by their inherent low electrical conductivity and large volume expansion during cycling[4]. SnO₂ has a theoretical capacity of approximately 790 mA h g⁻¹, with SnLi_x (0 ≤ x ≤ 4.4) intermediate phases formed through the cycling process[5]. Nevertheless, the large volume

variation (≥ 250%) during alloying/dealloying processes was one of the obvious disadvantages of tin-based oxides, eventually leading to severe electrode pulverization and poor electrochemical performance[6]. To overcome this issue, tin-based oxides were often combined with carbonaceous materials[7], although the introduction of carbon materials, including graphene and carbon nanotubes, will not only reduce the total energy density, but also lower the initial coulombic efficiency of the whole electrode.^[8] ZnO has a high theoretical capacity of approximately 978 mA h g⁻¹ and low volume variation (~109 %) for LIBs, which can ensure the integrity of the electrode structure, although cracking or fracturing was observed at points of high strain in the reacting interface through in-situ testing, indicating that ZnO has poor plasticity.^[9] In this context, ZnSnO₃, combining the advantages of ZnO and SnO₂, has been considered as one of the most promising candidates for LIBs, owing to its larger theoretical capacity (1317 mAh g⁻¹), better electrical conductivity (SnO₂: 1.3 × 10² S cm⁻¹, ZnSnO₃: 2.5 × 10² S cm⁻¹), moderate volume expansion (~191%), broad operating potential, element abundance, and

diverse morphology[10, 11]. Although ZnSnO_3 has been extensively studied for LIBs, its corresponding hydroxide, that is, $\text{ZnSn}(\text{OH})_6$ (ZSH) with a typical perovskite structure, has not been studied yet as an anode for LIBs[12].

In this work, the lithium storage capability of ZSH is reported for the first time. Uniform ZSH nanocubes (30–50 nm) were synthesized via a facile hydrothermal method, and they exhibited higher specific capacity and longer cycling lifespan than amorphous ZnSnO_3 (A-ZSO) anode for LIBs. The outstanding electrochemical performance of ZSH anode can be ascribed to the unique nano-cubic structure and the synergistic effects of Zn and Sn elements. Our results indicate that bi-metal hydroxides can also be a class of promising anodes for LIBs, which are comparable to bi-metal oxides or sulfides in electrochemical performance.

Experimental

Synthesis of uniform ZSH nanocubes

0.43 g $\text{Zn}(\text{Ac})_2 \cdot 2\text{H}_2\text{O}$ was dissolved into 15 mL de-ionized (DI) water under continuous stirring, and then, 1.2 g sodium citrate was added. After that, 15 mL of $0.13 \text{ mol L}^{-1} \text{ K}_2\text{SnO}_3 \cdot 3\text{H}_2\text{O}$ solution was added into the above solution. The mixture was then transferred into a 50 mL Teflon-lined stainless-steel autoclave and heated at 180°C for 12 h. The final product was separated by centrifugation and washed with DI water and ethanol several times, and then dried at 80°C overnight in a vacuum oven. The obtained material was marked as ZSH.

By contrast, another sample was prepared by the same procedure without adding sodium citrate.

Synthesis of amorphous ZnSnO_3

The amorphous ZnSnO_3 (A-ZSO) was obtained by annealing ZSH at 450°C in argon.

Synthesis of ZnO and SnO_2

0.43 g $\text{Zn}(\text{Ac})_2 \cdot 2\text{H}_2\text{O}$ was first dissolved into 15 mL DI water. 0.64 g NaOH was added into the solution with continuous stirring, and then the mixture was transferred into a 50 mL Teflon-lined stainless-steel autoclave and heated at 180°C for 12 h.

0.59 g $\text{K}_2\text{SnO}_3 \cdot 3\text{H}_2\text{O}$ was dissolved into 15 mL DI water. After stirring for several minutes, a certain amount of urea was added into the solution, and then the mixture was transferred into a 50 mL Teflon-lined stainless-steel autoclave and heated at 200°C for 24 h.

Electrochemical measurements

In order to measure the electrochemical performance, the working electrode was fabricated by mixing the active material, acetylene black carbon powder, and sodium carboxymethyl cellulose (CMC) powder in a weight ratio of 7: 2: 1. The mixture was then mixed with DI water to form a homogeneous slurry, which was then uniformly coated on the surfaces of copper substrates and dried at 100°C for 12 h in a vacuum oven. The CR2025 cells were fabricated in a glove box

(SG1200/750TS-H) filled with argon, and the electrolyte was 1 M LiPF_6 in a 1: 1: 1 (volume ratio) mixture of ethyl carbonate (EC), diethyl carbonate (DEC), and dimethyl carbonate (DMC). Li foil was used for the counter electrodes. The galvanostatic charge-discharge tests were conducted on a Land battery measurement system (Wuhan, China), and the voltage range was 0.01 – 3 V vs. Li/Li^+ at room temperature. The cyclic voltammetry (CV) curves and electrochemical impedance spectra (EIS) were collected on an electrochemical workstation (CHI 660d).

Characterization

The obtained materials were characterized by X-ray diffraction (XRD) with $\text{Cu K}\alpha$ radiation at a scanning rate of 5° min^{-1} (D/MAX-IIIC, Rigaku, Japan). The morphologies of the samples were investigated by field emission scanning electron microscopy (SEM, JEOL JSM-7500FA). X-ray photoelectron spectroscopy (XPS) was conducted on an ESCALAB 250Xi photoelectron spectrometer using monochromatic $\text{Al K}\alpha$ radiation under vacuum at $2 \times 10^{-6} \text{ Pa}$. The thermal properties of the as-prepared samples were characterized by thermogravimetric analysis (TGA; DIAMOND TG/DTA, PERKIN ELMER, USA) under N_2 atmosphere over a temperature range of 30– 800°C with a heating rate of $20^\circ\text{C min}^{-1}$. Fourier transform infrared spectroscopy (FT-IR) was conducted on a MAGNA-IR 750 (NICOLET iS10, USA).

Results and discussion

The crystal structures and chemical compositions of the obtained products could be measured by X-ray diffraction (XRD). As shown in Fig. 1a, all the peaks of the XRD diffraction patterns of ZSH can be well matched with $\text{ZnSn}(\text{OH})_6$ (JCPDS No.20-1445), and the distinct diffraction peaks indicate that they are well-crystallized. The inset of Fig. 1a describes ZSH as belonging to the class of perovskite-structured hydroxides, whose metal atoms are octahedrally coordinated with oxygen atoms to form $\text{Zn}(\text{OH})_6$ and $\text{Sn}(\text{OH})_6$ polyhedra, and these polyhedra share common oxygen atoms to construct the structural framework[13]. By contrast, the A-ZSO obtained by calcinating ZSH shows a broad diffraction peak at approximately 33.5° , corresponding to amorphous ZnSnO_3 [10, 14]. In addition, the XRD diffraction pattern of a sample obtained without sodium citrate is displayed in Fig. S1 in the Supporting Information, but it was composed of $\text{ZnSn}(\text{OH})_6$ and Zn_2SnO_4 [15]. FT-IR investigations were carried out to further investigate the structure of the products, as is shown in Fig. 1b. The broad peak at around 3220 cm^{-1} reflects the bending and stretching vibrations of -OH groups in ZSH. The four bands at around 540 cm^{-1} , 665 cm^{-1} , 1175 cm^{-1} , and 2339 cm^{-1} are attributed to the vibrations of the M (metal)-OH or M-OH-M groups in ZSH. The peak of A-ZSO at $\sim 1540 \text{ cm}^{-1}$, which is very weak after calcination is attributed to the vibrations of adsorbed water[16]. Peaks

for vibrations of M-O or M-O-M groups in A-ZSO are observed at $\sim 585\text{ cm}^{-1}$ and 1110 cm^{-1} . The peak at $\sim 3425\text{ cm}^{-1}$ in the spectrum of A-ZSO can be attributed to the physical adsorption of H_2O molecules on the surface [17]. Moreover, the peaks of the -OH groups in the samples nearly disappeared after calcination, while the peaks of metal-oxygen bonds at around $500\text{--}600\text{ cm}^{-1}$ became enhanced. These results indicate that the ZSH consists of M-OH and M-OH-M groups, while the A-ZSO contains M-O and M-O-M groups. The thermal behavior of ZSH was investigated through thermogravimetric (TG) analysis (Fig. 1c). The ZSH underwent a sharp weight loss between 200°C and 400°C , and retained 79.6% of its original weight under N_2 atmosphere, which is quite close to the theoretical weight loss of 81.1% to form ZnSnO_3 . As the temperature continued to rise, no further weight loss was observed, indicating the complete decomposition of the ZSH and the simultaneous formation of A-ZSO above 400°C [18].

In order to investigate the relationship between the mechanical properties and the electrochemical properties of ZSH, stress-strain tests were carried out. For comparison, ZnO and SnO_2 were also synthesized, and the corresponding XRD patterns are shown in Fig. 1d and Fig. 1e. The ZSH, ZnO, and SnO_2 were respectively mixed with DI water in the same proportions to form a homogenous slurry, and then cut into the same shape after drying, with a thickness of about $30\ \mu\text{m}$, width of 15 mm , and length of 27 mm . The selected tensile curves (Fig. 1f) corresponding to the useful part of the specimens are quite different, indicating that the ZSH has better plasticity than ZnO and SnO_2 . The detailed experimental results obtained from stress-strain measurements are summarized in Table 1.

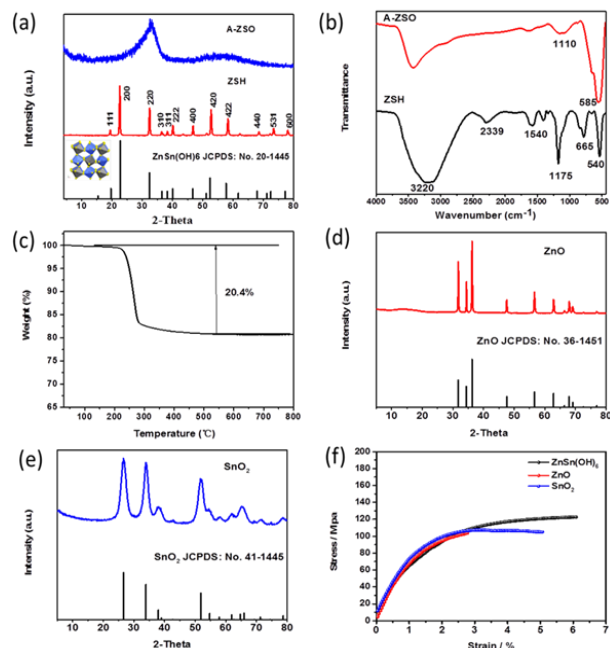


Fig. 1. (a) X-ray diffraction patterns of the two samples and the standard card; (b) FTIR spectra of the ZSH and A-ZSO, respectively; (c) TG curves of ZSH; (d, e) X-ray diffraction patterns of the ZnO, SnO_2 and the standard cards; (f) Typical nominal tensile stress-strain curves of ZSH, ZnO and SnO_2 , respectively.

Table 1. Results of the stress-strain measurements.

Sample	Elongation at break (%)	Tensile strength (MPa)
ZnSn(OH)_6	6.09	122.91
ZnO	2.78	103.21
SnO_2	5.06	105.76

The XPS survey spectrum of the ZSH cubes demonstrates that the sample primarily includes Zn^{2+} , Sn^{4+} , and O^{2-} (Fig. 2a). There are two major peaks with binding energies at 1022.9 and 1045.7 eV (Fig. 2b), which correspond to the binding energies of Zn $2p_{3/2}$ and Zn $2p_{1/2}$ [19]. Two strong peaks at around 495.1 and 486.7 eV (Fig. 2c) are assigned to Sn $3d_{3/2}$ and Sn $3d_{5/2}$, and the values correspond to the binding energies of the Sn^{4+} ion [20]. The peak of O 1s at 531.5 eV (Fig. 2d) corresponds to the -OH within the ZnSn(OH)_6 and adsorbed -OH, and the other one at around 530.2 eV is assigned to the oxygen in metal oxide (e.g. Sn-O-Zn) [21]. The ratio of Sn : Zn : O given by the quantification of peaks is 7.27 : 8.36 : 49.39, indicating that the molar ratio of Sn : Zn : O is near 1 : 1 : 6, which is close to the stoichiometric ratio of pure ZnSn(OH)_6 [22].

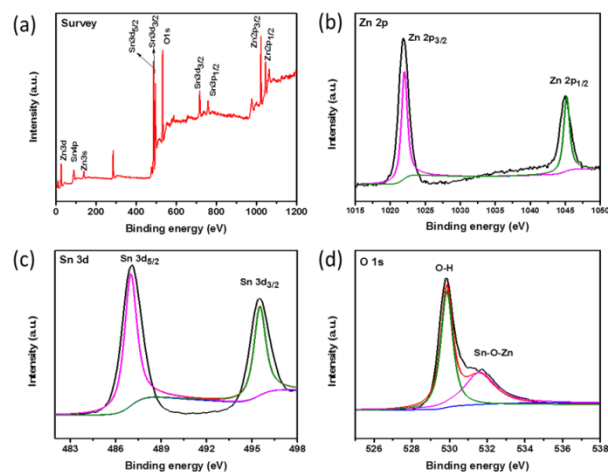


Fig. 2. XPS spectra of ZnSn(OH)_6 nanocubes: (a) Survey spectrum; (b) Zn region; (c) Sn region; (d) O region.

The microstructure of the samples was examined by field-emission scanning electron microscopy (FE-SEM). Uniform ZSH cubic crystallites ($30\text{--}50\text{ nm}$) can be observed in Fig. 3a. After annealing (Fig. 3b), however, the size of the cube-like A-ZSO particles increased to approximately 100 nm .

When compared with the ZSH, the particle shapes and the morphology of the sample without sodium citrate are irregular, and two different morphologies (sheet-like and cubic-like) are displayed in Fig. S2. Fig. 3c and Fig. 3d show typical transmission electron microscope (TEM) images of ZSH. A single cube of ZSH can be seen in Fig. 3c and Fig. 3d, which possesses a relatively smooth surface. High-resolution TEM (HRTEM) images and the corresponding fast Fourier transform-electron diffraction (FFT-ED) pattern of ZSH are shown in Fig. 3e and Fig. 3f. The corresponding inverse FFT (IFFT)-ED pattern (Fig. 3g) generated from Figure 3e

manifests lattice fringes with a spacing of 0.273 nm, which is in good agreement with the exposed {220} crystal facets of cubic $\text{ZnSn}(\text{OH})_6$.

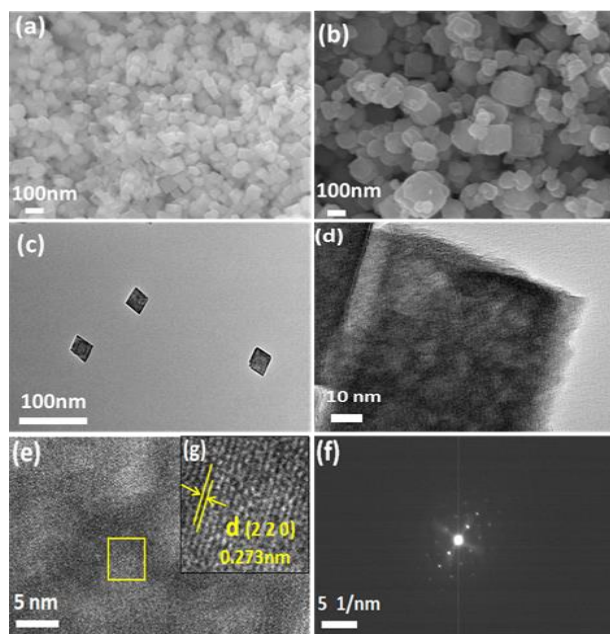


Fig. 3. (a, b) SEM images of ZSH and A-ZSO, respectively; TEM images of ZSH (c, d), with the corresponding inverse FFT (IFFT)-ED patterns (e, f and g), respectively.

Cyclic voltammetry (CV) curves of the $\text{ZnSn}(\text{OH})_6$ cubes and the A-ZSO are displayed in Fig. S3(a, b), and the first two cycles of the two samples are displayed in **Fig. 4a**. For ZSH, in the first cycle, there are one inconspicuous cathodic peak at ~ 1.3 V and two main cathodic peaks located at 0.05 and 0.43 V, owing to the multistep electrochemical lithiation process with the formation of the solid electrolyte interphase (SEI) layer, the initial reduction of $\text{ZnSn}(\text{OH})_6$ to metallic Zn and Sn, the further alloying phases of Li_xZn and Li_ySn , and the generation of LiOH [23], [24]. The two main anodic peaks located at about 0.68 and 1.12 V could correspond to the delithiation processes of Li_xSn and Li_yZn , and the decomposition of LiOH[25]. The weak anodic peak at about 1.59 V could correspond to the oxidation of Sn and Zn[26]. In the case of the A-ZSO, the two main cathodic peaks located at 0.13 and 0.46 V were attributed to the formation of alloys, Li_2O , and the SEI layer. The delithiation processes of Li_xSn and Li_yZn , and the decomposition of Li_2O were similar to what occurs in ZSH. The CV curves of the following 2nd and 5th cycles of the ZSH matched very well, indicating that the electrode has good electrochemical reversibility.

In order to research the electrochemical properties of the samples, the cycling performances of the samples were investigated under the same test conditions. **Fig. 4b** and **Fig. 4c** shows the discharge/charge profiles of the ZSH and A-ZSO at 500 mA g^{-1} in the potential window of 0.01 – 3.0 V. The initial discharge and charge capacities of ZSH (**Fig. 4b**) were 1585.8 and $986.7 \text{ mA h g}^{-1}$, respectively. There is a big capacity loss in the second cycle, however, which is attributed to the

initial irreversible formation of LiOH, the inevitable formation of the solid electrolyte interphase (SEI) layer, and electrolyte decomposition[27]. The discharge/charge profiles of the sample prepared without sodium citrate are displayed in Fig. S4, and the initial discharge and charge capacities was 1360.8 and $941.4 \text{ mA h g}^{-1}$, respectively. Compared with amorphous ZnSnO_3 and the sample prepared without sodium citrate (Fig. S5a), the ZSH exhibited better long-term cycling stability and better capacity retention (**Fig. 4d**). The first cycle coulombic efficiency (CE) of ZSH was about 62.3%, and the average coulombic efficiency was almost 100% from the second cycle, manifesting better stabilization of the SEI layer and of the structure of the whole electrode. It was found that the capacities of the A-ZSO and the sample prepared without sodium citrate decreased rapidly at 500 mA g^{-1} , and dropped quickly from 625.8 to $345.9 \text{ mA h g}^{-1}$ and 476.3 to $268.2 \text{ mA h g}^{-1}$ after 50 cycles, respectively. For ZSH, a capacity of $599.3 \text{ mA h g}^{-1}$ can still be retained after 200 cycles, manifesting the long lifespan of the cell based on ZSH nanocubes.

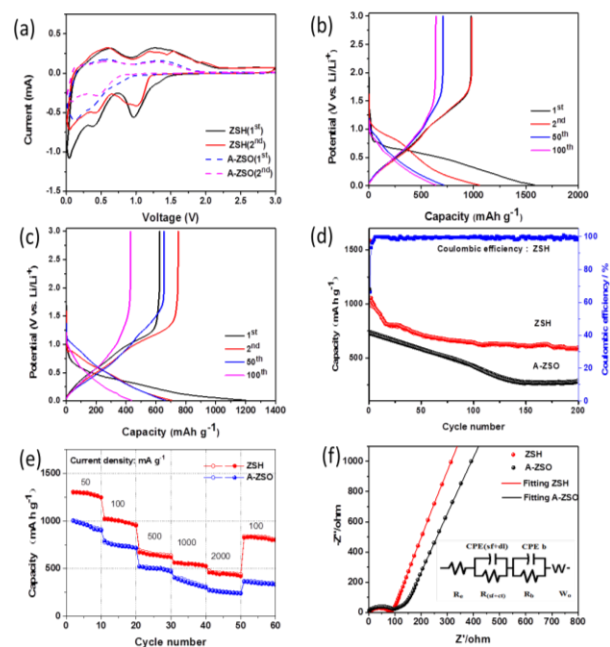


Fig. 4. Electrochemical performance: (a) Cyclic voltammograms of the first two cycles of ZSH and A-ZSO with the potential window from 0.01 V to 3.0 V; (b,c) Galvanostatic charge-discharge profiles of ZSH and A-ZSO for selected cycles at a current density of 0.5 A g^{-1} with the potential window from 0.01 V to 3.0 V; (d) Cycling performances of ZSH and A-ZSO at the charge/discharge current density of 0.5 A g^{-1} ; (e) Rate performance of ZSH and A-ZSO at the discharge/charge current densities of 0.05, 0.1, 0.5, 1 and 2 A g^{-1} ; (f) EIS spectra of ZSH and A-ZSO, with the inset showing the equivalent circuit.

The rate capability of these samples was measured at different current densities of 50, 100, 500, 1000, 2000, and 100 mA g^{-1} . Compared with the A-ZSO and the sample prepared without sodium citrate, the ZSH exhibited a high capacity of 1248.9, 854.1, 639.9, 526.1, 478.5, and $809.7 \text{ mA h g}^{-1}$ at these different current densities, respectively (**Fig. 4e** and Fig. S5b). Electrochemical impedance spectroscopy (EIS)

measurements of the ZSH and A-ZSO anodes were carried out. An equivalent electrical circuit model was used to fit the Nyquist plots (Figure 4f), which were each composed of one semicircle in the high and medium frequency region and a sloping line in the low-frequency region. In the equivalent circuit, R_e is the electrolyte resistance; $R_{(sf+ct)}$ is the resistance corresponding to the surface film and charge transfer; R_b is the bulk resistance; and W_o is the Warburg resistance. On the basis of the fitted results, the value of $R_{(sf+ct)}$ for ZSH was 76.33 Ω , which is lower than that for A-ZSO (99.08 Ω) [28].

These results indicate that the ZSH electrode possesses much better electrochemical properties and rate capacity than the A-ZSO. Firstly, relatively small particles (30–50 nm) of ZnSn(OH)₆ can extend the electrode/electrolyte contact area, which can accelerate the electron/ion transfer rate. Secondly, relatively good mechanical properties can stabilize the whole electrode during the Li⁺ extraction/insertion process. Moreover, the interlaced charge-discharge voltage platform can effectively buffer the volume expansions during the cycling process and stabilize the whole electrode.

Conclusion

In summary, ZSH nanocubes have been successfully synthesized by a facile and mild hydrothermal method, and their electrochemical performance in LIBs was studied for the first time. When applied as an anode material, the ZSH electrode exhibited a discharge capacity of 599.3 mA h g⁻¹ after 200 cycles at the current density of 500 mA g⁻¹, and it exhibited a discharge capacity of 526.1 mA h g⁻¹ even at 1 A g⁻¹. Moreover, the coulombic efficiency was almost 100% from the second cycle. The enhanced electrochemical performance might be due to its relatively small particles (30–50 nm), relatively good mechanical properties, and its interlaced charge-discharge voltage platform. Thus, the ZSH bi-metal hydroxide has great potential for advanced LIB application.

Acknowledgements

Financial support provided by a grant from the National Natural Science Foundation of China (No. 21476063), and the Australian Research Council (ARC) through an ARC Discovery project (DP170102406) are gratefully acknowledged. The authors would also like to thank Dr. Tania Silver for critical reading of the manuscript and valuable remarks.

Author's contributions

Conceived the plan: Qian Yang, Zhibin Wu, Zaiping Guo; Performed the experiments: Qian Yang, Zhijian Wang, Wei Liu; Data analysis: Qian Yang, Zhibin Wu, Jianwen Liu, Chuanqi Feng, Haimin Zhao, Wei Sun, Wrote the paper: Qian Yang, Zhibin Wu, Zaiping Guo. Authors have no competing financial interests.

Supporting information

Supporting informations are available from VBRI Press.

References

- (a) Y. Sun, N. Liu, Y. Cui, *Nature Energy* **2016**, *1*, 16071; (b) B. Dunn, H. Kamath, J.-M. Tarascon, *Science* **2011**, *334*, 928; (c) T. Sasaki, Y. Ukyo, P. Novák, *Nature Materials* **2013**, *12*, 569.
- (a) H. Wang, Y. Wu, Y. Bai, W. Zhou, Y. An, J. Li, L. Guo, *Journal of Materials Chemistry* **2011**, *21*, 10189; (b) Z. Wang, Z. Wang, W. Liu, W. Xiao, X. W. D. Lou, *Energy & Environmental Science* **2013**, *6*, 87.
- C. K. Chan, H. Peng, G. Liu, K. McIlwrath, X. F. Zhang, R. A. Huggins, Y. Cui, in *Materials For Sustainable Energy: A Collection of Peer-Reviewed Research and Review Articles from Nature Publishing Group*, World Scientific, **2011**, 187.
- Z. Jiang, Z.-J. Jiang, T. Maiyalagan, A. Manthiram, *Journal of Materials Chemistry A* **2016**, *4*, 5877.
- [5] M. Gao, X. Chen, H. Pan, L. Xiang, F. Wu, Y. Liu, *Electrochimica Acta* **2010**, *55*, 9067.
- a) X. Zhou, L. Yu, X. W. D. Lou, *Advanced Energy Materials* **2016**, *6*; b) Z. Yang, S. Zhao, W. Jiang, X. Sun, Y. Meng, C. Sun, S. Ding, *Electrochimica Acta* **2015**, *158*, 321.
- a) B.-Y. Wang, H.-Y. Wang, Y.-L. Ma, X.-H. Zhao, W. Qi, Q.-C. Jiang, *Journal of Power Sources* **2015**, *281*, 341; b) Y. Wang, D. Li, Y. Liu, J. Zhang, *Materials Letters* **2016**, *167*, 222; c) J. G. Kim, S. H. Nam, S. H. Lee, S. M. Choi, W. B. Kim, *ACS Applied Materials & Interfaces* **2011**, *3*, 828.
- a) Y. Li, S. Zhu, Q. Liu, J. Gu, Z. Guo, Z. Chen, C. Feng, D. Zhang, W.-J. Moon, *Journal of Materials Chemistry* **2012**, *22*, 2766; b) C. Zhang, X. Peng, Z. Guo, C. Cai, Z. Chen, D. Wexler, S. Li, H. Liu, *Carbon* **2012**, *50*, 1897.
- A. Kushima, X. H. Liu, G. Zhu, Z. L. Wang, J. Y. Huang, J. Li, *Nano Letters* **2011**, *11*, 4535.
- Y. Wang, D. Li, Y. Liu, J. Zhang, *Electrochimica Acta* **2016**, *203*, 84.
- F. Han, W. C. Li, C. Lei, B. He, K. Oshida, A. H. Lu, *Small* **2014**, *10*, 2637.
- L. Han, J. Liu, Z. Wang, K. Zhang, H. Luo, B. Xu, X. Zou, X. Zheng, B. Ye, X. Yu, *CrystEngComm* **2012**, *14*, 3380.
- X. Fu, X. Wang, Z. Ding, D. Y. Leung, Z. Zhang, J. Long, W. Zhang, Z. Li, X. Fu, *Applied Catalysis B: Environmental* **2009**, *91*, 67.
- Y. Ma, Q. Xie, X. Liu, Y. Zhao, D. Zeng, L. Wang, Y. Zheng, D.-L. Peng, *Electrochimica Acta* **2015**, *182*, 327.
- [15] X. Guo, M. Cai, R. Li, X. Han, *CrystEngComm* **2016**, *18*, 6608.
- a) F. Cheng, K. Huang, S. Liu, J. Liu, R. Deng, *Electrochimica Acta* **2011**, *56*, 5593; b) F. Huang, X. Lu, Y. Liu, J. Liu, R. Wu, *Materials Science and Technology* **2011**, *27*, 29.
- C. Chen, X. Zheng, J. Yang, M. Wei, *Physical Chemistry Chemical Physics (PCCP)* **2014**, *16*, 20073.
- J. Shao, Z. Wan, H. Liu, H. Zheng, T. Gao, M. Shen, Q. Qu, H. Zheng, *Journal of Materials Chemistry A* **2014**, *2*, 12194.
- L. Zou, X. Xiang, M. Wei, F. Li, D. G. Evans, *Inorganic Chemistry* **2008**, *47*, 1361.
- Y. Wang, T. Chen, *Electrochimica Acta* **2009**, *54*, 3510.
- H. Fan, S. Ai, P. Ju, *CrystEngComm* **2011**, *13*, 113.
- L. Wang, K. Tang, Z. Liu, D. Wang, J. Sheng, W. Cheng, *Journal of Materials Chemistry* **2011**, *21*, 4352.
- Y. Chen, B. Qu, L. Mei, D. Lei, L. Chen, Q. Li, T. Wang, *Journal of Materials Chemistry* **2012**, *22*, 25373.
- a) L. Qin, S. Liang, X. Tan, A. Pan, *Journal of Alloys and Compounds* **2017**, *692*, 124; b) M. Marcinek, L. Hardwick, T. Richardson, X. Song, R. Kostecki, *Journal of Power Sources* **2007**, *173*, 965.
- R. Zhang, Y. He, L. Xu, *Journal of Materials Chemistry A* **2014**, *2*, 17979.
- a) N. Du, H. Zhang, B. Chen, J. Wu, X. Ma, Z. Liu, Y. Zhang, D. Yang, X. Huang, J. Tu, *Advanced Materials* **2007**, *19*, 4505; b) Y. Sharma, N. Sharma, G. Subba Rao, B. Chowdari, *Advanced Functional Materials* **2007**, *17*, 2855.
- a) Y. Qi, N. Du, H. Zhang, P. Wu, D. Yang, *Journal of Power Sources* **2011**, *196*, 10234; b) X. Guo, X. Fang, Y. Sun, L. Shen, Z. Wang, L. Chen, *Journal of Power Sources* **2013**, *226*, 75.
- a) W. Liu, T. Zhou, Y. Zheng, J. Liu, C. Feng, Y. Shen, Y. Huang, Z. Guo, *ACS Applied Materials & Interfaces* **2017**, *9*, 9778; b) M. Jiang, T. Zhou, W. Liu, C. Feng, J. Liu, Z. Guo, *RSC Advances* **2017**, *7*, 17769.

Supplementary materials

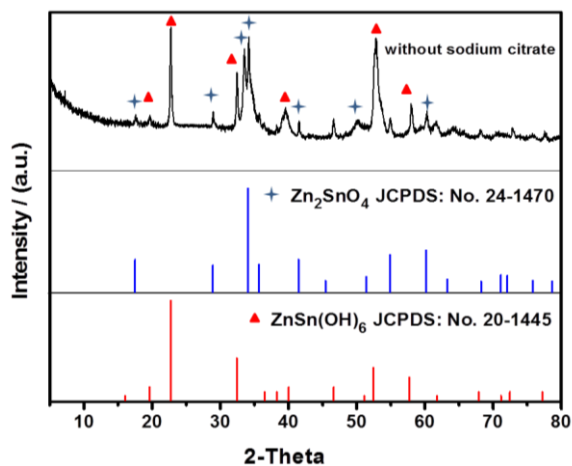


Fig.S1 X-ray diffraction patterns of the sample prepared without sodium citrate;

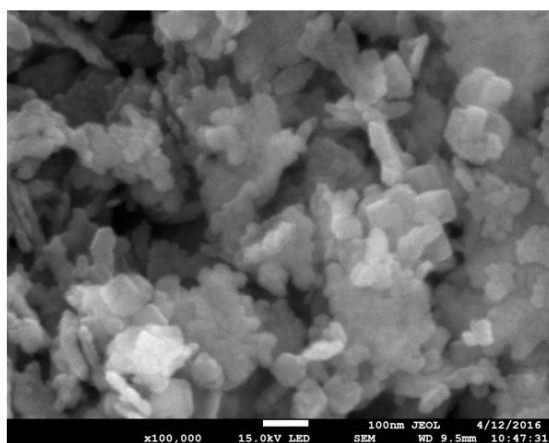


Fig.S2 SEM images of the sample prepared without sodium citrate;

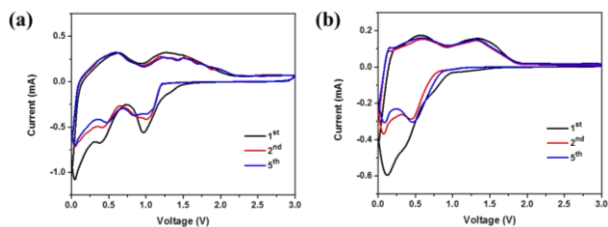


Fig.S3 (a) Cyclic voltammograms of ZSH with the potential window from 0.01 V to 3.0 V; (b) Cyclic voltammograms of A-ZSO with the potential window from 0.01 V to 3.0 V;

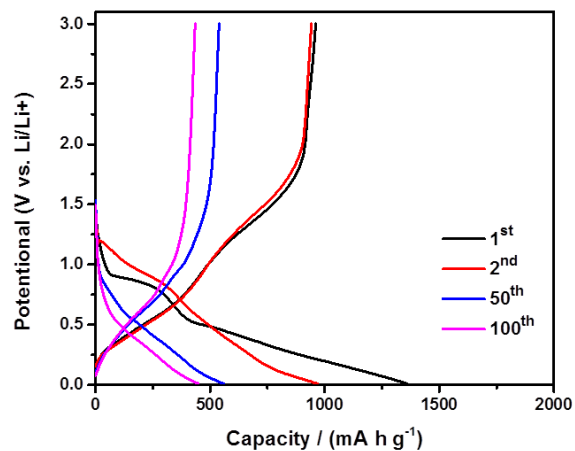


Fig.S4 Galvanostatic charge-discharge profiles of the sample prepared without sodium citrate for selected cycles at a current density of 0.5 A g⁻¹ with the potential window from 0.01 V to 3.0 V;

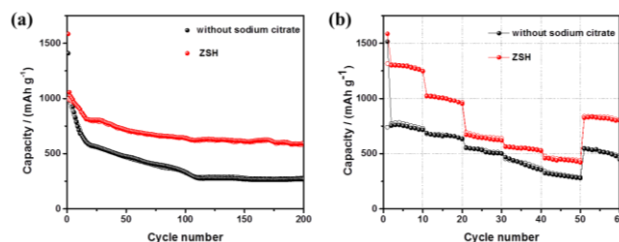


Fig.S5 (a) Cycling performances of the sample prepared without sodium citrate and ZSH at the charge/discharge current density of 0.5 A g⁻¹; (b) Rate performance of the sample prepared without sodium citrate and ZSH at the discharge/charge current densities of 0.05, 0.1, 0.5, 1 and 2 A g⁻¹;